Chemical Geology 658 (2024) 122122

Contents lists available at ScienceDirect

Chemical Geology

journal homepage: www.elsevier.com/locate/chemgeo

How does the burial rate control the diagenesis of sandstone? Insights from a diagenetic physical simulation experiment

Sirui Chen [a,b], Benzhong Xian [a,b,*], Youliang Ji [a,b], Jiaqi Li [c], Naveed Ur Rahman [b], Rongheng Tian [b], Pengyu Wang [b]

[a] National Key Laboratory of Petroleum Resources and Engineering, China University of Petroleum (Beijing), Beijing 102249, China
[b] College of Geosciences, China University of Petroleum (Beijing), Beijing 102249, China
[c] School of Energy Resources, China University of Geosciences, Beijing 100083, China

ARTICLE INFO

Editor: Claudia Romano

Keywords:
Burial rate
Diagenesis
Overpressure
Sandstone reservoirs
Physical simulation experiment

ABSTRACT

The study conducted physical simulation experiments on sandstone samples from the Junggar Basin to investigate how burial rates influence sandstone diagenesis and reservoir quality. Results show that the mechanical compaction under a negative burial rate (tectonic uplift) almost stops to destroy the sandstone reservoir space, the capacity of fluid seepage is the strongest and the sandstone tends to develop 'weak compaction–strong dissolution' diagenetic facies. For positive burial rates, sandstones with a low burial rate tend to develop 'medium compaction–medium dissolution' diagenetic facies; sandstones at a medium burial rate easily form 'strong compaction–weak dissolution' diagenetic facies, and sandstones at a high burial rate tend to develop 'weak compaction–weak dissolution' diagenetic facies. Experimental results indicate that the compaction strength and damage to sandstone reservoirs may not consistently rise with the burial rate. Faster burial rates do not always intensify compaction; the degree of compaction depends on fluid overpressure. If the increase in burial rate does not induce the fluid overpressure in sandstones, the burial rate is higher and the destruction degree of primary pores caused by mechanical compaction is greater; mechanical compaction also simultaneously causes the diagenetic system to be more closed and the dissolution to be weaker. If the increase in burial rate can induce the fluid overpressure in sandstones, the burial rate is higher, the inhibition of mechanical compaction by fluid overpressure is more pronounced. However, fluid overpressure also strengthens the closure of the diagenetic system, hindering the injection of external acidic fluids into the sandstone, which is not conducive to dissolution. Overall, low burial rates with normal pressure favour secondary pore development, high burial rates with overpressure preserve primary pores, while medium burial rates with normal pressure are unfavourable for primary and secondary pores.

1. Introduction

As an essential reservoir for oil and gas resources, sandstones have long been the focus of research on clastic rocks in sedimentary basins (Bloch et al., 2002; Morad et al., 2010). The degree of preservation of primary pores and the development of secondary pores in sandstones are critical factors for their reservoir performance (Dixon et al., 1989; Dutton and Loucks, 2010; Yuan et al., 2017a). Currently, the impact of sediment type, mineral composition, and fluid activity on sandstone diagenesis has been extensively investigated (Bjørlykke and Jahren, 2012; Worden et al., 2016; Yuan et al., 2017b; Hansen et al., 2021; Fu et al., 2022), but there is still a lack of research on how burial rates control sandstone diagenesis.

As a vital variable during sandstone subsidence, its potential influence on diagenesis must not be ignored (Curtis, 1980; Leder and Park, 1986; Saha and Bhattacharya, 2022). In different petroliferous basins, different tectonic backgrounds and tectonic subsidence rates lead to different burial processes or styles in their sandstone reservoirs. Through the observation of burial histories in rift basins, foreland basins and craton basins, we found that stratigraphic burial rates are as low as a few meters (Karimi et al., 2016; Aschwanden et al., 2019), as medium as tens of meters/million years (Salama et al., 2021) and as high as hundreds of meters/million years (Sathar and Jones, 2016; Chen et al., 2017). When the stratum undergoes tectonic uplift, the burial depth decreases rather

* Corresponding author at: National Key Laboratory of Petroleum Resources and Engineering, China University of Petroleum (Beijing), Beijing 102249, China.
E-mail address: xianbzh@cup.edu.cn (B. Xian).

https://doi.org/10.1016/j.chemgeo.2024.122122
Received 17 December 2023; Received in revised form 28 February 2024; Accepted 28 April 2024
Available online 30 April 2024

than increases, and the burial rate is negative. Some scholars believe that the faster the burial rate is, the greater the intensity of mechanical compaction is and the higher the damage to the primary pores of sandstones is (Sun et al., 2013); however, there are also arguments that the faster the burial rate is, the greater the probability of fluid overpressure development is, which is more favourable to the inhibition of mechanical compaction (Sathar and Jones, 2016; Baig et al., 2019). In addition to mechanical compaction, the relationship between burial rate and dissolution has been frequently discussed. Let us take the example of organic acids and meteoric freshwater, common in sandstones. Some scholars believe that the higher the burial rate, the more likely that organic acids will decompose, which is unfavourable to the development of secondary pores; on the contrary, it is conducive to the preservation of organic acids (Chen et al., 2017; Wang et al., 2020). Generally, there are also arguments that the faster the burial rate is, the more likely it is to generate fluid overpressure, and the primary pores of sandstone protected by overpressure can theoretically serve as the charging space for organic acids, which is conducive to the enrichment of organic acids (Jin et al., 2018). For meteoric freshwater, some scholars think that tectonic uplift is an excellent opportunity for the intrusion of meteoric freshwater into sandstones (França et al., 2003; Baruch et al., 2015). However, suppose the sandstone enters the rapid deep burial stage too early. In that case, it will reduce the possibility of meteoric freshwater entering the sandstone, likely inhibiting early dissolution and aggravating the blockage of primary pores caused by siliceous cementation (Poursoltani et al., 2019).

Therefore, although many studies have confirmed that burial rate changes can influence the diagenesis of sandstone, there are still many contradictions and controversies between these research conclusions. The results of the literature investigation show that the mechanical compaction intensity can obtain either an improvement or inhibition in the background of an increasing burial rate; similarly, this experience may be either favourable or unfavourable for dissolution. This situation indicates that current studies are still unclear regarding the diagenetic response mechanisms of sandstone under different burial rates. Simultaneously, the recent interpretations of the diagenetic responses at different burial rates are dominated by qualitative descriptions and the lack of quantitative evidence to support them, which restricts the understanding of the role played by different burial rates in diagenetic evolution. In addition, it is challenging to distinguish diagenetic phenomena with varying burial rates from present-day core samples by relying only on traditional experimental means, which leads to a decrease in the accuracy of research conclusions.

Diagenetic physical simulation experiments have the advantages of visualisation and quantification, which are effective methods used to explain diagenetic mechanisms. Previous studies have explored the factors that influence the intensity of mechanical compaction and dissolution using physical simulation experiments (Chuhan et al., 2002; Xi et al., 2015). For mechanical compaction, physical simulation experiments are used more often to discuss the influence of grain size, sorting, and rock compositions on the intensity of mechanical compaction (Xi et al., 2015; Yang et al., 2016; Qu et al., 2020), but rarely involve burial rates. For dissolution, physical simulation experiments are mainly used to analyse fluid-rock interactions (Ma et al., 2022). However, in the actual underground environment, both mechanical compaction and dissolution usually coexist in sandstone reservoirs. Therefore, dissolution simulation experiments in a lack of mechanical compaction environments may difficult to contribute to the interpretation of dissolution mechanisms in actual reservoirs.

In view of the above research status and problems, we plan to conduct diagenetic physical simulation experiments under dynamic variations in temperature, pressure and diagenetic fluids. We aim to establish the connection between low, medium, high and negative burial rates (tectonic uplift) and sandstone diagenesis and to answer the following key questions: (1) what are the response characteristics of mechanical compaction and dissolution of sandstones at different burial rates? (2) In what mechanisms do different burial rates influence sandstone diagenesis, and what factors play a determinative role? (3) What is the significance of different burial rates on sandstone reservoir quality? (4) What is the contribution of this study to sandstone reservoir prediction in regions with complicated burial histories? Finally, we aim to provide a reference example for applying physical simulation techniques in the diagenetic field.

2. Samples and methods

2.1. Experimental materials

The samples used for this physical simulation experiment are unconsolidated sands from the modern outcrop area at the southern margin of the Junggar Basin. When discussing the effect of burial rate on mechanical compaction, it is necessary to exclude the interference of particle size on the experimental results. Thus, we measured the percentage of each particle size in unconsolidated sands, which was 14.7% for coarse sands, 27.2% for medium sands, 47.8% for fine sands and 10.8% for silt sands. Then, the coarse, medium, fine and silty sands in unconsolidated sands are successively screened out by the three-dimensional vibrating screen. Considering the limited space of the reaction furnace, each group of experiments was assigned 11 g of silt sand, 48 g of fine sand, 27 g of medium sand and 15 g of coarse sand. This method excludes the effect of particle size on the experimental results and ensures the same mass of unconsolidated sand in each group of experiments.

In addition to mechanical compaction, this study will discuss the impact of burial rate on dissolution. X-Ray Diffraction(XRD) results show that the unconsolidated sand contains 50.8% quartz, 17.4% potassium feldspar, 7.2% plagioclase feldspar, 10.9% calcite, 8.2% montmorillonite and 3.4% illite, which provides adequate dissolvable objects for physical simulation experiments and makes it easy to observe and compare the differences in dissolution characteristics under different burial rates. Under the premise that the amount of dissolvable minerals is sufficiently guaranteed, the acidic fluid becomes a critical factor in the dissolution simulation. This study simulates the most representative acidic fluid in sandstones–meteoric freshwater and organic acids. The CO_2 (g) was continuously injected into pure water and reacted adequately with pure water to make a carbonic acid solution (H_2CO_3) with a pH of 5.2, which was used to simulate meteoric freshwater. Acetic acid is a common organic acid in oilfield water. This article configured an acetic acid solution (CH_3COOH) with pH 3.8 to simulate organic acids.

2.2. Experimental procedures

The diagenetic physical simulation equipment is independently designed and constructed by the Petroleum Geology Research and Laboratory Centre of the Research Institute of Petroleum Exploration and Development (Yang et al., 2016). This modelling system consists of a pressure supply module, a fluid supply and collection module, a central computer control module and six reaction furnaces (Fig. 1).

To differentiate between burial rate levels, they were categorized as low (10 m/h: the simulated burial rate is a few meters/million years), medium (50 m/h: the simulated burial rate is tens of meters/million years), and high (250 m/h: the simulated burial rate is hundreds of metres/million years), respectively. Considering that sandstone reservoirs are distributed in both shallow and deep layers, the simulation experiments in this study are conducted in three parts. The experiments in part 1 (groups 1, 2, 3) were used to investigate how different burial rates control the diagenesis of shallow sandstones. Shallow layers are defined internationally as having a burial depth of less than 2.8 km (Glasmann, 1992). The present study, 2.0 km was selected as the maximum simulation depth of the shallow layer, and meteoric freshwater was selected as the acidic fluid to participate in the dissolution

Fig. 1. Reservoir diagenesis modelling system used for the physical simulation experiment. (A) Six parallel reaction furnaces. (B) Pressure pump module. (C) Fluid supply and collection module. (D) Central computer control module.

reaction (Table 1). The experiments in part 2 (groups 4, 5, 6) were used to analyse how different burial rates control the diagenesis of deep sandstones. 4.0–6.0 km is internationally defined as the range of burial depths in deep layers (Dutton and Loucks, 2010; Sun et al., 2013). The current study, 6.0 km was selected as the maximum simulation depth of the deep layer. When the simulated depth exceeded the shallow depth (2.0 km), we injectd organic acids into the reaction furnace (Table 1). The experiment in part 3 was used to investigate the control of the negative burial rate (tectonic uplift) on sandstone diagenesis (group 7). When the simulation depth reaches 2.0 km, the temperature and pressure in the reaction furnace begin to decrease until both reach the temperature and pressure conditions corresponding to 1.0 km (Fig. 3C, F). The burial rate of the group 7 experiment is set at 10 m/h, and the acidic fluid that participates in the dissolution reactions is also meteoric freshwater (Table 1).

The following are the experimental steps in this diagenetic physics simulation. Configured unconsolidated sands were thoroughly mixed with an appropriate amount of distilled water (Fig. 3A). After 24 h of standing, the soaked, unconsolidated sands were poured into copper tubes to be sealed and then placed in the reaction furnace (Fig. 3B, C). Prior to commencing the experiments, a consistent temperature increase of 25 °C and a uniform lithostatic pressure increase of 27.5 MPa per 1000 m of simulated depth were programmed into the central computer module (Fig. 2). Simultaneously, to ensure that the experimental results at the time scale of diagenetic physical simulation are more closely related to diagenetic phenomena at the time scale of real geological time, the temperature and pressure values of each group of experiments were compensated. Considering that the compensation value must not impair the regular operation of the experimental equipment, the compensation value of temperature was decided to be 200 °C, and the compensation value of lithostatic pressure was 55 MPa (Fig. 2). Finally, the diagenetic physical simulation equipment was activated to experiment.

After the experiments, the ion concentrations of the experimental fluids from each reaction vessel were analysed using inductively coupled plasma mass spectrometry. The following analyses were performed on the cylindrical sandstone samples (Fig. 3): (1) observing the mineral morphology using an optical microscope and scanning electron microscope; (2) combining the optical microscope and image analysis software to calculate the surface porosity of thin sections; (3) obtaining the pore and permeability data of the cylindrical samples with the aid of gas porosity and permeability metres and (4) obtaining the maximum pore throat radius (R_{Max}), the pore throat radius of moderate saturation pressure level (R_{50}) and the average pore radius (Rt) of the cylindrical samples by using pressure-controlled mercury injection.

3. Results

3.1. Diagenetic phenomenon

The detrital particles from sample #1 are mainly in point-line contact (Fig. 4A). Primary pores with regular morphology are most commonly distributed around detrital particles (Fig. 4A). Concurrently, both feldspar and calcite have undergone significant dissolution and generated secondary pores (Fig. 4B, C).

The detrital particles from sample #2 are mainly in line contact. The distribution area of primary pores is small (Fig. 4D). The dissolution intensity is weak, and the distribution area of calcite is large (Fig. 4D).

The detrital particles from sample #3 are predominantly in point contact. A small number of particles are not even in contact (Fig. 4E). The distribution area of primary pores is extremely large. Part of calcites are obviously dissolved (Fig. 4F).

The detrital particle contact relationship from sample #4 includes point-line and line contacts, and the primary pore distribution area is

Table 1
Parameter design of diagenetic physical simulation experiments.

Group No.							Simulated depth /km	Temperature/°C	Lithostatic pressure /MPa	Main fluid	
1	2	3	4	5	6	7					
Burial rate (m/h)											
10	50	250	10	50	250	10					
Simulated time (day)										Shallow layer	Deep layer
2.10	0.52	0.08	2.10	0.52	0.08	2.10	0.5	212.5	68.75	Meteoric freshwater	Deionized water
4.20	1.04	0.17	4.20	1.04	0.17	4.2 (9.0)	1.0	225	82.5		
6.20	1.56	0.25	6.20	1.56	0.25	6.20	1.5	237.5	96.25		
8.30	2.08	0.33	8.30	2.08	0.33	8.30	2.0	250	110		
			10.42	2.60	0.42		2.5	262.5	123.75		
			12.50	3.13	0.50		3.0	275	137.5		
			14.58	3.65	0.58		3.5	287.5	151.25		
	/		16.67	4.17	0.67		4.0	300	165	/	Organic acid
			18.75	4.69	0.75		4.5	312.5	178.75		
			20.83	5.21	0.83		5.0	325	192.5		
			22.92	5.73	0.92		5.5	337.5	206.25		
			25.00	6.25	1.00		6.0	350	220		

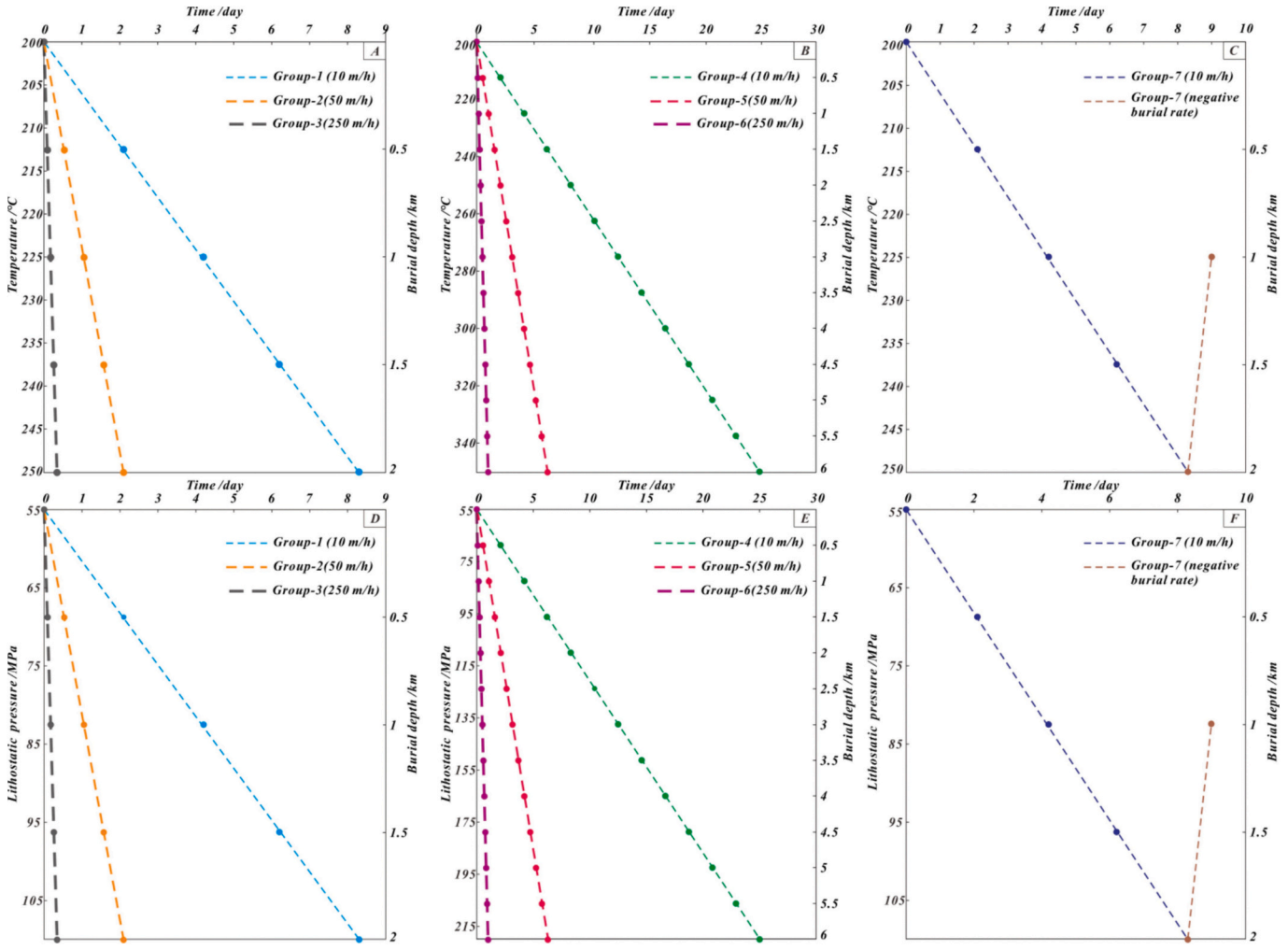

Fig. 2. The characteristics of temperature and lithostatic pressure in each group of experiments.

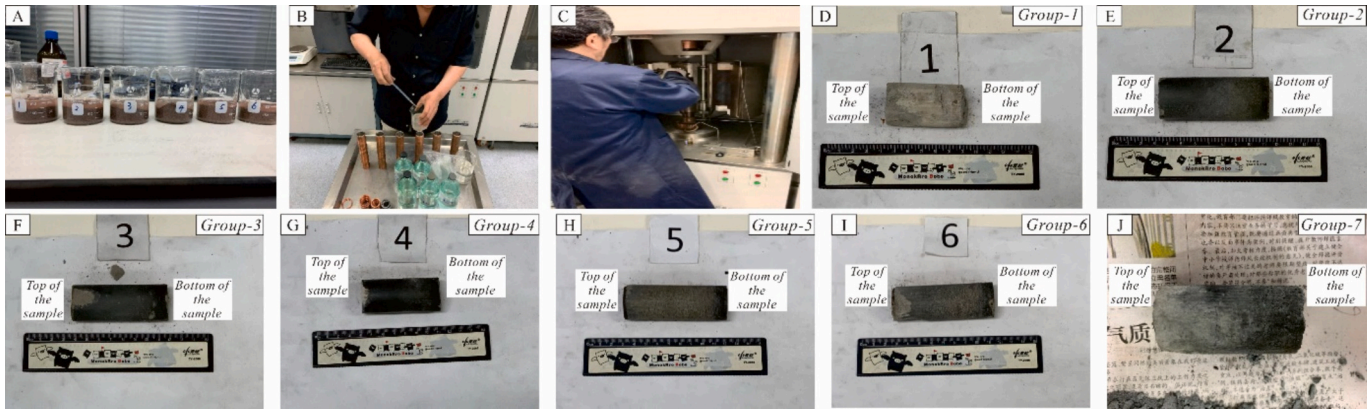

Fig. 3. (A) Unconsolidated sands before the experiments. (B—C) The process of loading unconsolidated sands into the reactive furnaces. (D) Sample #1 (Group-1, 10 m/h). (E) Sample #2 (Group-2, 50 m/h). (F) Sample #3 (Group-3, 250 m/h). (G) Sample #4 (Group-4, 10 m/h). (H) Sample #5 (Group-5, 50 m/h). (I) Sample #6 (Group-6, 250 m/h). (J) Sample #7 (Group-7, negative burial rate).

small (Fig. 4G). Feldspar dissolution pores can be observed in the thin section (Fig. 4H).

The detrital particles from sample #5 are dominated by line and concave contacts, and the primary pores are almost lost (Fig. 4I). Feldspar and calcite are almost not dissolved (Fig. 4J). Authigenic kaolinite was observed to precipitate in the primary pores under a scanning electron microscope.

The detrital particles from sample #6 are dominated by point-line contacts, and the distribution of primary pores is large (Fig. 4L). Secondary pores due to feldspar and calcite dissolution are observed in thin sections (Fig. 4M, N).

The detrital particles from sample #7 are predominantly in point

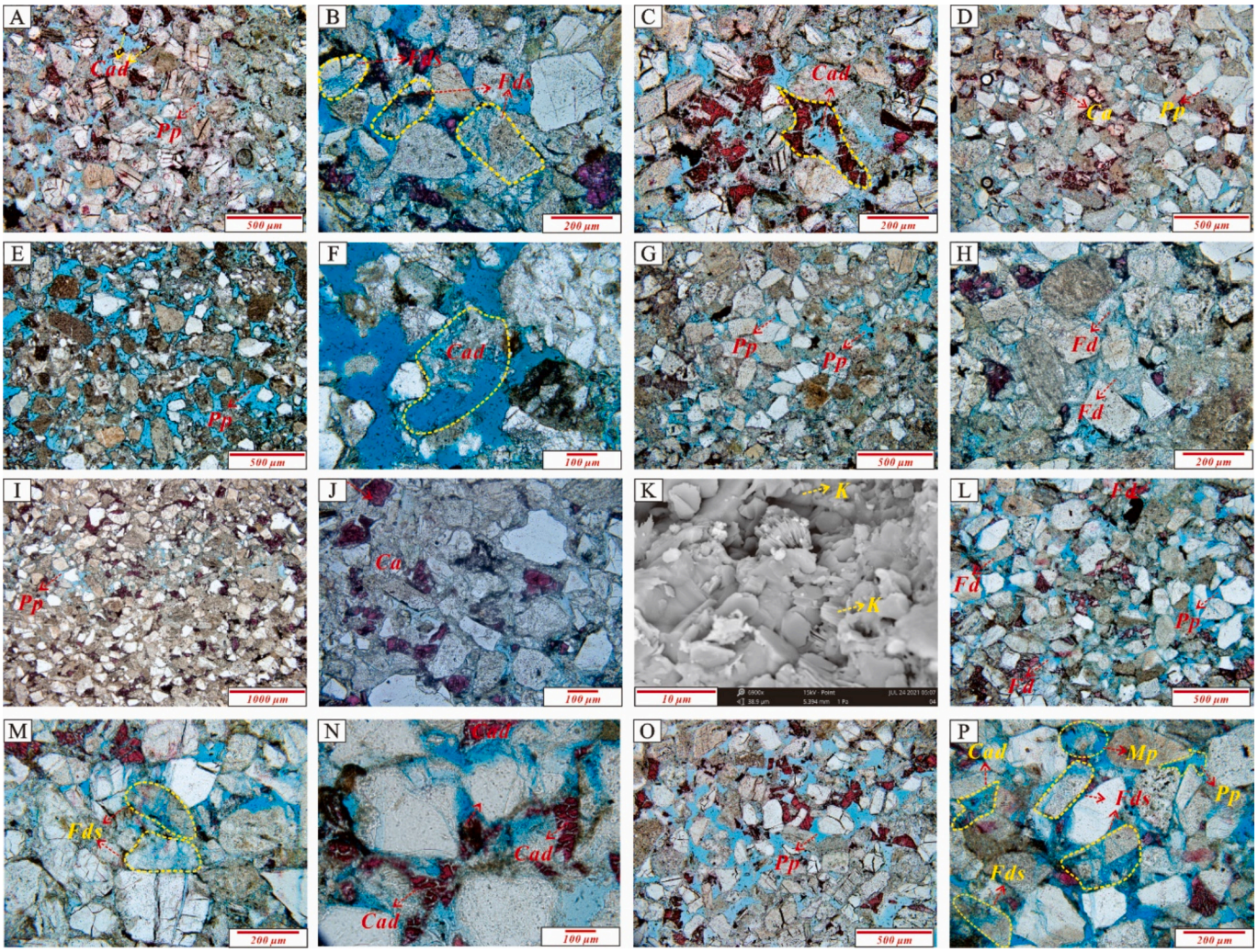

Fig. 4. Microscopic characteristics of seven cylindrical sandstone samples. (A) Detrital particles are mostly in point-line contact, and the primary pores are well-developed (Sample #1, PPL). (B) The dissolution of feldspar is obvious (Sample #1, PPL). (C) The dissolution of calcite is obvious (Sample #1, PPL). (D) Detrital particles are mostly in linear contact, and the distribution area of calcites is large (Sample #2, PPL). (E) Detrital particles are mostly in point contact, and the distribution area of the primary pore is very large (Sample #3, PPL). (F) Calcite is dissolved (Sample #3, PPL). (G) Detrital particles are mostly in point-line to linear contact (Sample #4, PPL). (H) Some feldspar is weakly dissolved (Sample #4, PPL). (I) Detrital particles are mostly in linear to concavo-convex contact (Sample #5, PPL). (J) Feldspar and calcite are not dissolved (Sample #5, PPL). (K) Kaolinite precipitates in primary pores (Sample #5, PPL). (L) Detrital particles are mostly in point-line contact, and the distribution area of primary pore is large (Sample #6, PPL). (M) Feldspar particles are dissolved and secondary pores are formed (Sample #6, PPL). (N) Calcite is dissolved (Sample #6, PPL). (O) Detrital particles are mostly in point contact, and the distribution area of primary pore is large (Sample #7, PPL). (P) Some feldspar particles are almost completely dissolved (Sample #7, PPL). PPL: plane-polarized light; Pp: primary pore; Mp: mould pore; Cad: calcite dissolution; Fds: feldspar dissolution; K: kaolinite.

contact, and the distribution area of primary pores is large (Fig. 4O). Both feldspar and calcite were strongly dissolved, and some feldspar dissolved entirely and formed mould pores (Fig. 4P).

3.2. Reservoir space

The surface porosity of sample #1 is 7.4%, the primary surface porosity is 5.3% and the secondary surface porosity is 2.1%. Sample #2 has a 5.2% surface porosity, consisting of 4.1% primary and 1.1% secondary surface porosity. Sample #3 has 9.2% surface porosity, with 8.8% primary and 0.4% secondary surface porosity. Sample #4 has a 4.2% surface porosity, 2.9% primary surface porosity, and 1.3% secondary surface porosity. Sample #5 has a surface porosity of 1.3%, a primary surface porosity of 1.2%, and a secondary surface porosity of 0.1%. The surface porosity of sample #6 is 7.2%, the primary surface porosity is 6.5%, and the secondary surface porosity is 0.7%. Sample #7 has a 9.6% surface porosity, consisting of 6.4% primary surface porosity and 3.2% secondary surface porosity (Fig. 5).

3.3. Physical property and pore-throat

Sample #1 has a porosity of 27.6% and a permeability of 30.8 mD (Fig. 6). The maximum pore throat radius (R_{Max}) is 6.76 μm, the pore throat radius of moderate saturation pressure level (R_{50}) is 1.74 μm and the average pore throat radius (R_t) is 1.33 μm (Fig. 7).

Sample #2 has a porosity of 23.3% and a permeability of 18.8 mD (Fig. 6). The maximum pore throat radius is 5.34 μm, the pore throat radius of moderate saturation pressure level is 1.33 μm and the average pore radius is 1.15 μm (Fig. 7).

Sample #3 has a porosity of 30.1% and a permeability of 66.3 mD (Fig. 6). The maximum pore throat radius is 11.41 μm, the pore throat radius of moderate saturation pressure level is 3.07 μm and the average pore radius is 2.15 μm (Fig. 7).

Sample #4 has 16.3% porosity and 12.2 mD permeability (Fig. 6).

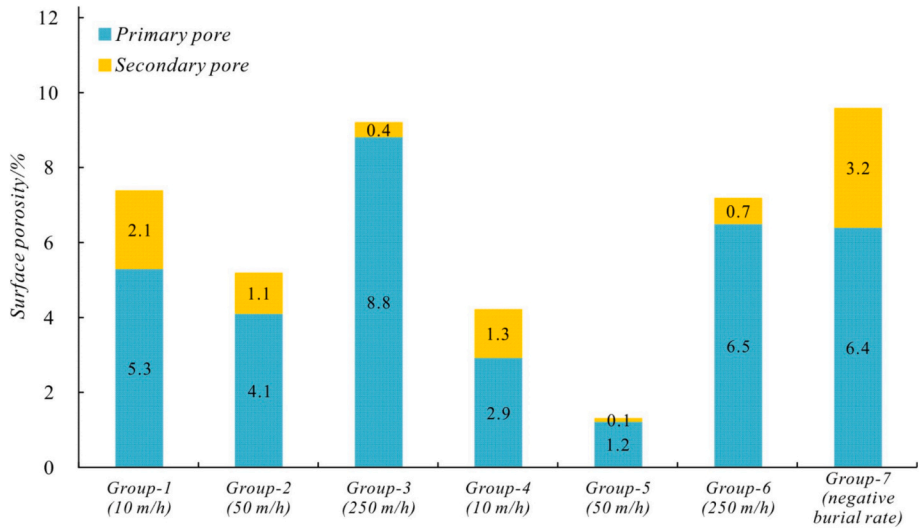

Fig. 5. Distribution characteristics of primary and secondary pore content in seven cylindrical sandstone samples.

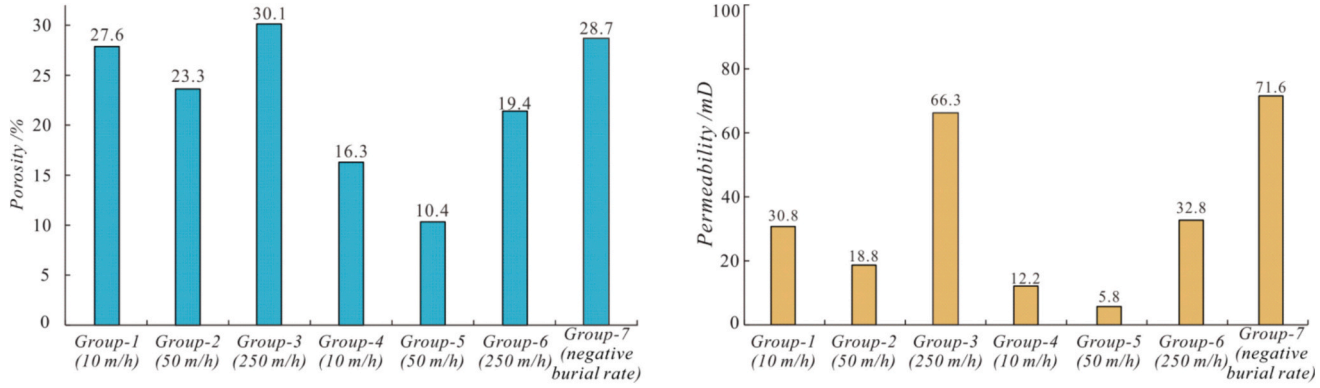

Fig. 6. Distribution characteristics of porosity and permeability in seven cylindrical sandstone samples.

The maximum pore throat radius is 2.34 μm, the pore throat radius of a moderate saturation pressure level is 0.68 μm and the average pore radius is 0.58 μm (Fig. 7).

Sample #5 showed a porosity of 10.4% and a permeability of 5.8 mD (Fig. 6). The maximum pore throat radius is 1.33 μm, the pore throat radius of a moderate saturation pressure level is 0.38 μm and the average pore radius is 0.23 μm (Fig. 7).

Sample #6 has a porosity of 19.4% and a permeability of 32.8 mD (Fig. 6). The maximum pore throat radius is 7.41 μm, the pore throat radius of a moderate saturation pressure level is 1.63 μm and the average pore radius is 1.29 μm (Fig. 7).

Sample #7 has a porosity of 28.7% and a permeability of 71.6 mD (Fig. 6). The maximum pore throat radius is 13.83 μm, the pore throat radius of a moderate saturation pressure level is 3.42 μm and the average pore radius is 2.85 μm (Fig. 7).

3.4. Fluid chemistry

Group 1 experiment has fluid concentrations of Ca^{2+}, K^{+}, Na^{+}, Al^{3+} and SiO_2 (aq) of 45.1, 255, 1514, 0.46 and 117 mg/L, respectively. Group 2 experiment has fluid concentrations of 29.7, 130, 337, 0.36 and 127 mg/L for Ca^{2+}, K^{+}, Na^{+}, Al^{3+} and SiO_2 (aq), respectively. Group 3 experiment has fluid concentrations of Ca^{2+}, K^{+}, Na^{+}, Al^{3+} and SiO_2 (aq) of 13.1, 5.12, 51.2, 0.14 and 28.6 mg/L, respectively. Group 4 experiment has fluid concentrations of 33.5, 191, 878, 0.36 and 70.8 mg/L for Ca^{2+}, K^{+}, Na^{+}, Al^{3+} and SiO_2 (aq), respectively. Group 5 experiment has the lowest concentrations of Ca^{2+}, K^{+}, Na^{+}, Al^{3+} and SiO_2 (aq), which are 14.4, 29.5, 218, 0.29 and 18.5 mg/L, respectively. Group 6 experiment has fluid concentrations of Ca^{2+}, K^{+}, Na^{+}, Al^{3+} and SiO_2 (aq) of 24.4, 93.1, 535, 0.32 and 53.3 mg/L, respectively. Group 7 experiment has fluid concentrations of Ca^{2+}, K^{+}, Na^{+}, Al^{3+} and SiO_2 (aq) of 80.8, 357, 1650, 0.55 and 212 mg/L, respectively (Fig. 8).

3.5. Fluid pressure

We recorded the pore fluid pressure changes in real-time for each group of experiments (Fig. 9). Then, we calculated the pressure coefficients corresponding to different fluid pressures using the empirical formula: $P = P_c \times D_s \times 0.0098$ (where P—fluid pressure, P_c—pressure coefficient, D_s—burial depth; Qu et al., 2020).

The pore fluid pressure of the group 1 experiment ranges from 4 to 19 MPa, and the pressure coefficient ranges from 0.8 to 1. The pore fluid pressure of the group 2 experiment ranges from 5 to 21 MPa, and the pressure coefficient is slightly greater than 1. The group 3 experiment has a pore fluid pressure interval of 6–29 MPa, and the pressure coefficient ranges from 1.2 to 1.5. The group 4 experiment has a pore fluid pressure interval of 5–64 MPa with pressure coefficients between 0.8 and 1.1. The group 5 experiment has a pore fluid pressure interval between 6 and 71 MPa, and the pressure coefficient ranges from 1.1 to 1.2. The pore fluid pressure interval of the group 6 experiment ranges from 6 to 106 MPa, and the pressure coefficient ranges from 1.3 to 1.8. The group 7 experiment has a pore fluid pressure interval of 4–19 MPa with

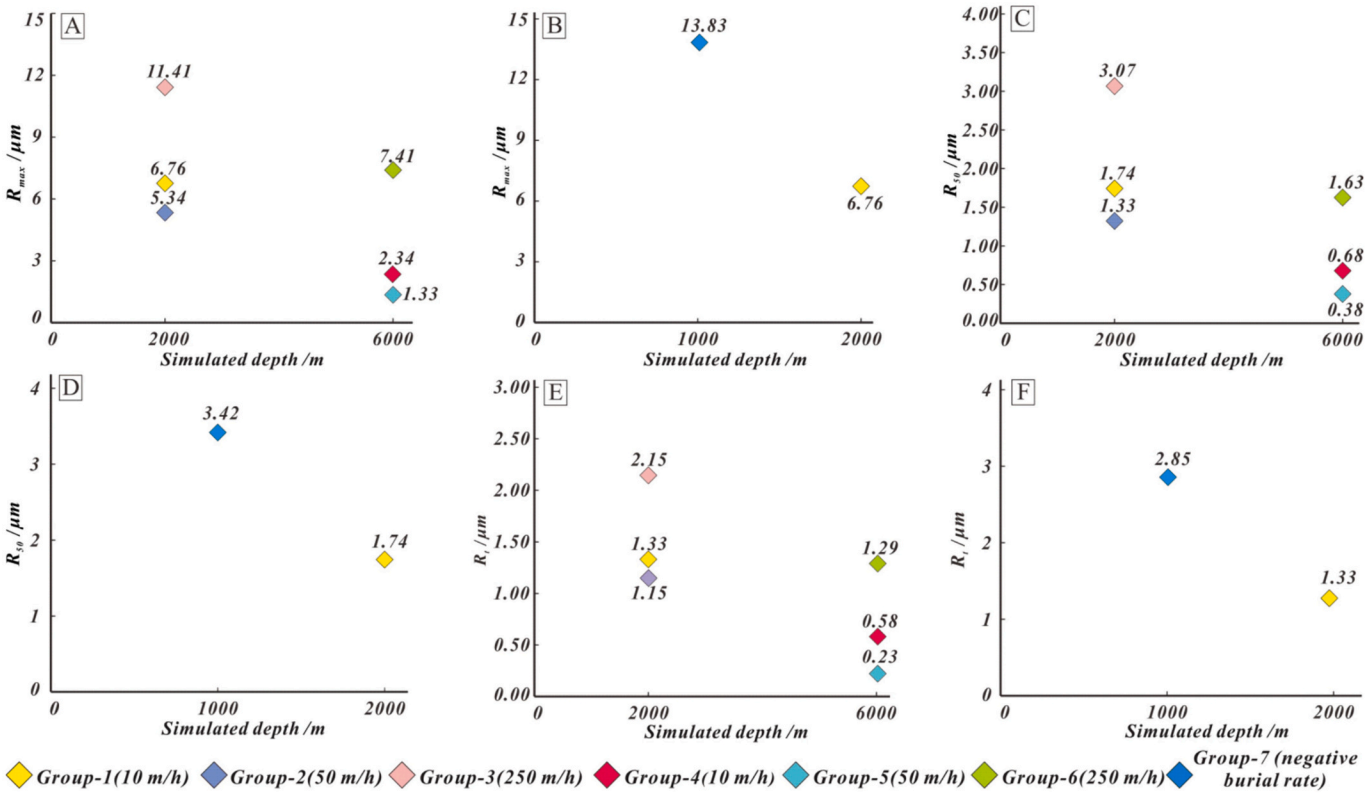

Fig. 7. Distribution characteristics of maximum pore throat radius (R_{Max}), pore throat radius of moderate saturation pressure level (R_{50}), and average pore throat radius (R_t) in seven cylindrical sandstone samples.

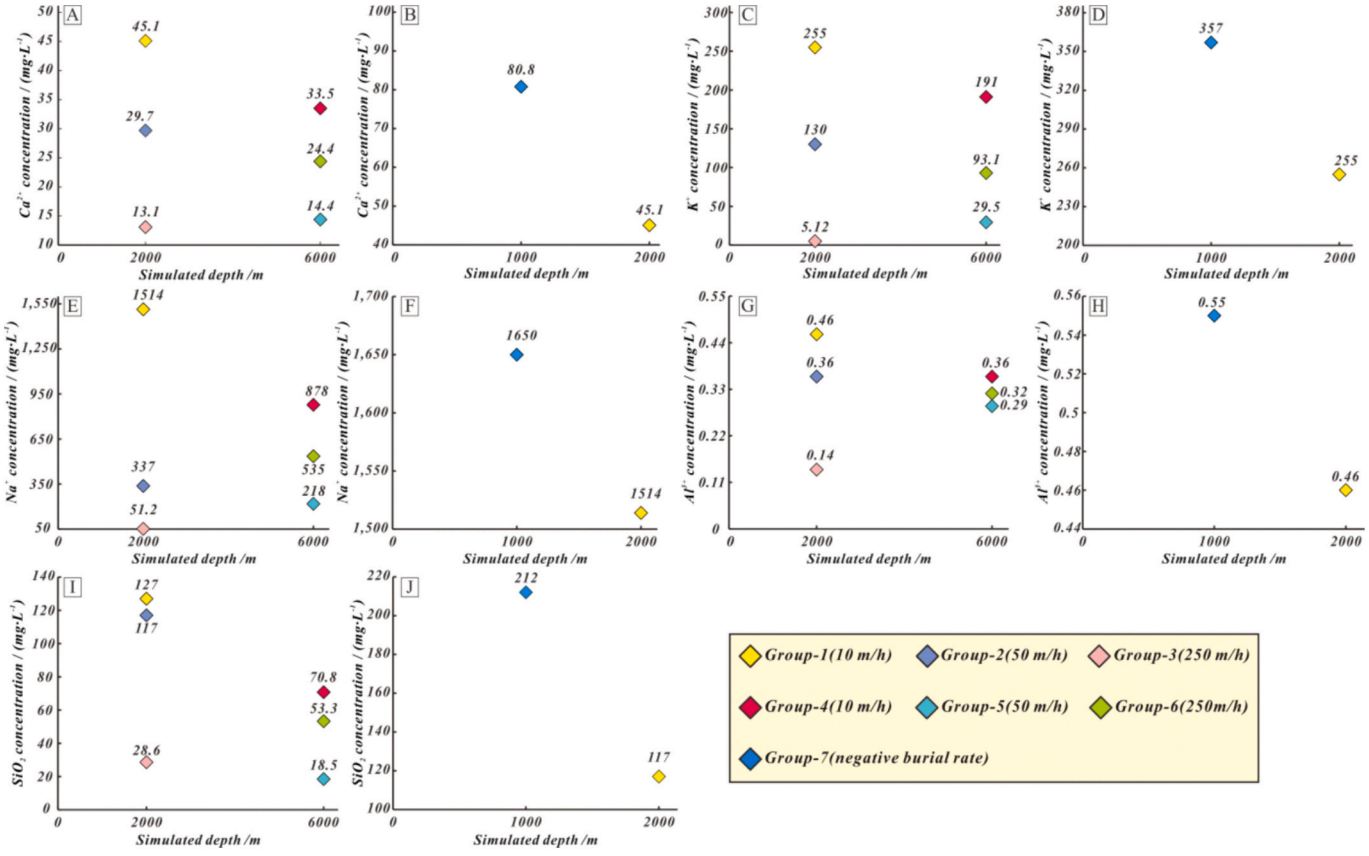

Fig. 8. The change characteristics of typical ion concentration in each group of experiments.

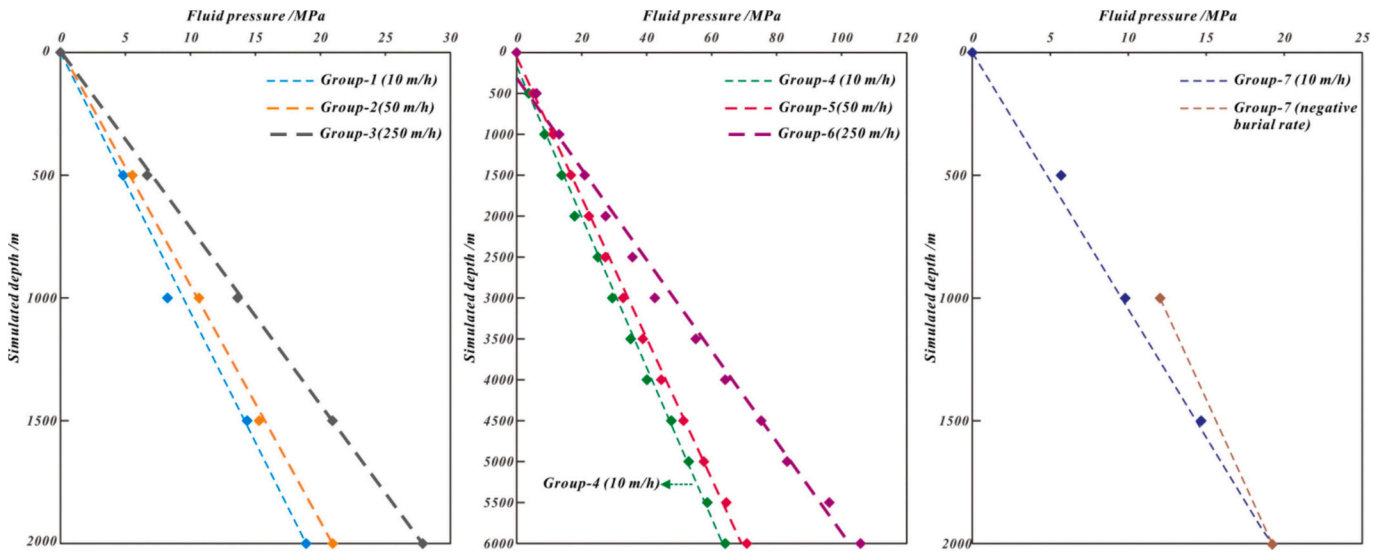

Fig. 9. The change characteristics of fluid pressure in each group of experiments.

pressure coefficients between 0.8 and 1.0 (Table 2).

4. Discussion

4.1. Influence of burial rate on mechanical compaction

4.1.1. High burial rate

Unburied detrital particles are rich in pore water, which acts as a 'natural barrier' preventing them from coming into contact with each other. Upon entering the burial stage, mechanical compaction will drive pore water out of the primary pores, resulting in more particles coming into contact with each other, leading to a decrease in the primary pore content (Hui et al., 2020; Teng et al., 2022). Pressure coefficients can indirectly reflect the status of pore water during the diagenetic process (Ma et al., 2020; Tenger et al., 2021). By comparing the experimental results of each group, we found significant differences in pressure coefficients under different burial rates. Pressure coefficients at low and medium burial rates remain at normal-pressure levels. In contrast, pressure coefficients at high burial rates reach overpressure–strong overpressure levels (Table 2). These experimental results demonstrate that a highly burial rate is most favourable for inhibiting pore water escape from the primary pore and maintaining high pore fluid pressures in the sandstone reservoirs (Fig. 9). The increase in fluid pressure causes a reduction in the vertical effective stress acting on the surface of the particles, which can alleviate the destruction of primary pores by mechanical compaction (Sathar and Jones, 2016; Wang et al., 2019). Based on the experimental results, the primary pore content of the shallow layer sandstone (2.0 km) at the high burial rate is 1.6 and 2.1 times higher than that at the low and medium burial rates, respectively (Fig. 5). The detrital particle contact relationship is mainly in point contacts (Fig. 4E). Compared to the shallow layer, the influence of high pore fluid pressure on the primary pore space is more significant at the deep layer (6.0 km). The experimental results show that the primary pore content of sandstones at a high burial rate is 2.2 and 5.4 times higher than that at low and medium burial rates, respectively (Fig. 5). The detrital particles are mainly in point-line contacts (Fig. 4L). In addition, high burial rates are extremely favourable for maintaining open-pore throats. Comparison of the experimental results of groups 1 and 4, groups 2 and 5 and groups 4 and 6 revealed that from shallow to deep, R_{Max}, R_{50} and R_t decreased by 35%, 47% and 40%, respectively, at high burial rates (Fig. 7A, C, E), which were significantly lower than those at low and medium burial rates.

Table 2
The values of fluid pressure and pressure coefficient in each group of experiments.

D /m	Pfp /MPa	Pc	D /m	Pfp /MPa	Pc	D /m	Pfp /MPa	Pc	D /m	Pfp /MPa	Pc
Group-1 (10 m/h)			*Group-2 (50 m/h)*			*Group-3 (250 m/h)*			*Group-7 (negative burial rate)*		
0	0	0	0	0	0	0	0	0	0	0.00	0.00
500	4.61	0.94	500	5.33	1.09	500	6.26	1.27	500	4.25	0.87
1000	8.23	0.84	1000	10.66	1.09	1000	13.62	1.39	1000	9.80	1.00
1500	14.36	0.98	1500	15.28	1.04	1500	20.93	1.42	1500	14.67	1.00
2000	18.90	0.96	2000	20.94	1.07	2000	27.87	1.42	2000	19.17	0.98
Group-4 (10 m/h)			*Group-5 (50 m/h)*			*Group-6 (250 m/h)*			1000	8.96	0.91
0	0	0	0	0	0	0	0	0			
500	5.05	1.03	500	5.90	1.20	500	6.10	1.24			
1000	8.61	0.88	1000	11.23	1.15	1000	13.08	1.34			
1500	13.85	0.94	1500	16.72	1.14	1500	20.94	1.42			
2000	17.87	0.91	2000	22.26	1.14	2000	27.41	1.40			
2500	25.03	1.02	2500	27.32	1.12	2500	35.64	1.45			
3000	29.45	1.00	3000	32.78	1.12	3000	42.55	1.45			
3500	35.13	1.02	3500	38.84	1.13	3500	55.14	1.61			
4000	40.11	1.02	4000	44.55	1.14	4000	64.20	1.64			
4500	47.61	1.08	4500	51.34	1.16	4500	75.30	1.71			
5000	52.95	1.08	5000	57.65	1.18	5000	83.27	1.70			
5500	58.70	1.09	5500	64.54	1.20	5500	96.25	1.79			
6000	64.20	1.09	6000	70.85	1.20	6000	105.86	1.80			

D-depth, Pfp-pore fluid pressure, Pc-pressure coefficient.

4.1.2. Low and medium burial rates

The pressure coefficients of the sandstones at low and medium burial rates are of the normal-pressure level, and the fluid pressure is no longer a critical factor in inhibiting mechanical compaction. According to the experimental results, detrital particles at low burial rates in shallow or deep layers are mainly in point-line contact (Fig. 4A, G). In contrast, detrital particles at medium burial rates are mainly in line contact and concave contact (Fig. 4D, I, J). Simultaneously, sandstones primary pore content and pore structure at low burial rates are superior to those at medium burial rates (Fig. 5; Fig. 7A, C, E). Therefore, when the burial depth is the same but the pore fluid pressure is at a normal-pressure level (Fig. 9; Table 2), the vertical stresses on the surface of detrital particles accumulate less at an extremely low burial rate than at a medium burial rate, and the mechanical compaction is weaker than at medium burial rates (Fig. 10).

4.1.3. Negative burial rate (tectonic uplift)

The experimental results show that the contact relationship of the detrital particle of the sandstone experiencing tectonic uplift (group 7) changed from point-line contact to point contact (Fig. 4O), with a 20% increase in primary pore content (Fig. 5) and an increase of more than 50% in R_{Max}, R_{50} and R_t (Fig. 7B, D, F). Previous studies have shown that strata suffering from denudation or tectonic uplift will cause a reduction in the vertical stress of the detrital particles, resulting in a 'rebound' of the compressed rock skeleton volume and causing an increase in pore volume (Parks and Tóth, 1995; Li et al., 2013; Li et al., 2019; Li et al., 2022). Combined with this experimental result, we believe that when the burial rate of the stratum is negative, mechanical compaction will stop temporarily destroying the reservoir space and pore structure. A large amount of sandstone sediment will be transformed from the 'extrusion state' to the 'diffusion state', and the primary pores that have been previously destroyed can be 'released' for a second time (Fig. 10). However, group 7 showed only a 1.1% increase in porosity compared to group 1. In contrast, permeability increased by 40.8 mD (Fig. 6). A comparison of the increased amplitudes of the physical property parameters reveals that the improvement in sandstone permeability caused by negative burial rates is much more significant than that in sandstone porosity, which has positive implications for the mobility of acidic fluid and dissolution. This subject will be carefully discussed in the following section.

4.2. Influence of burial rate on dissolution

4.2.1. High burial rate

Previous studies have shown that the mobility of pore water in sandstone will be inhibited in an overpressure environment (Osborne and Swarbrick, 1999; Bloch et al., 2002; Hao et al., 2002). Based on the experimental results, the pressure coefficients of sandstones at high burial rates always belong to the overpressure–strong overpressure level compared to the low and medium burial rates (Table 2). These experimental results mean that in the background of a high burial rate, the pore fluid pressure in the primary pores very quickly reaches the overpressure–strong overpressure level, which makes it difficult for subsequent acidic fluids to enter the sandstone to dissolve the unstable components. The experimental results of groups 1, 2 and 3 show that the sandstones at high burial rates have the lowest secondary pore content (Fig. 5), and the Ca^{2+}, K^{+}, Na^{+}, Al^{3+} and SiO_2 (aq) in the fluids are also at their lowest values (Fig. 8). Simultaneously, in the experimental results of groups 4, 5 and 6, the secondary pore content of sandstones and the ion concentration of fluids at high burial rates are also smaller than those at low burial rates and only slightly better than those at medium burial rates (Fig. 5; Fig. 8). Thus, the 'physical barrier' effect of fluid overpressure in sandstones on external fluids is significant, implying that even if sandstone sediments have good pore throat structures under a highly burial rate, it is difficult for external acidic fluids to enter the sandstone on a large scale to dissolve unstable minerals.

4.2.2. Low burial rate

The dissolution degree of unstable minerals is closely related to their equilibrium constants for chemical reactions (Yuan et al., 2017b). Previous work has demonstrated through numerical simulations that the equilibrium constant of chemical reactions will decrease with increasing temperature (Yuan et al., 2015a). The same acidic fluid dissolves less calcite and feldspar at higher temperatures than lower ones (Fig. 11, Cao et al., 2022). The 'low burial rate' has the advantage of slowing down the rate of increase in formation temperature, which helps calcite and

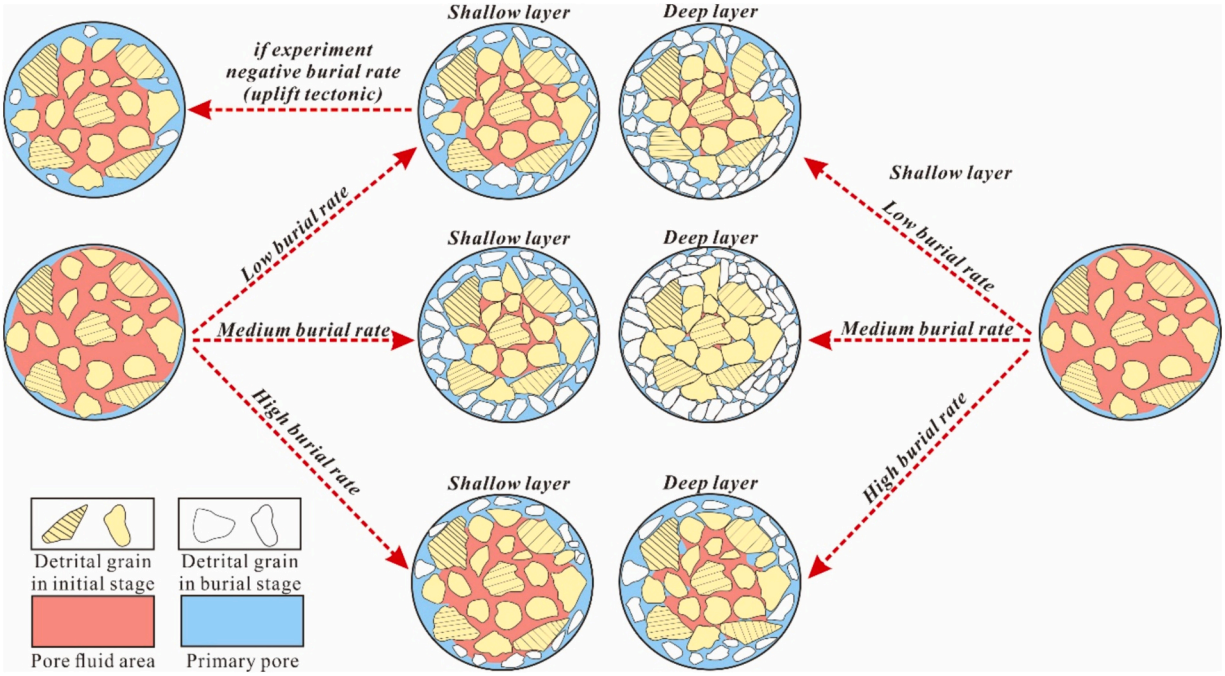

Fig. 10. Schematic diagram of influence of different burial rates on mechanical compaction of sandstone reservoirs.

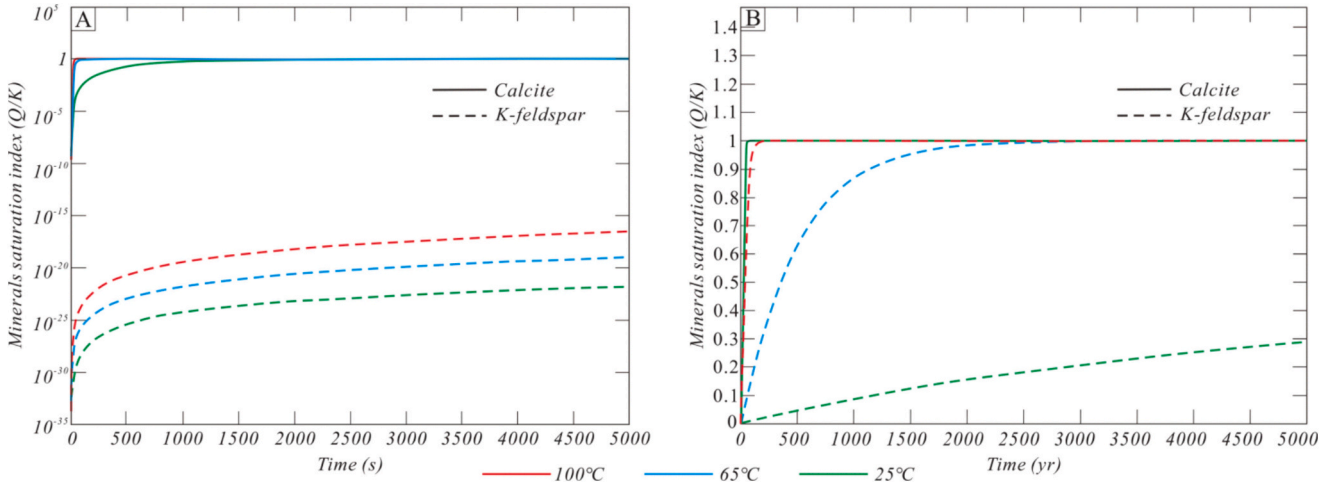

Fig. 11. Numerical simulation results of the dissolution of K-feldspar and calcite by CO_2-charged fluids at different temperatures (modified from Yuan et al., 2015a; Yuan et al., 2017b; Cao et al., 2022). (A) Short-term (5000 s) simulation results. (B) Long-term (5000 years) simulation results.

feldspar maintain high chemical reaction equilibrium constants, prolonging the time for dissolution–precipitation to reach equilibrium and allowing more minerals to be dissolved by acidic fluids. Concurrently, the pore throat structure of sandstone at a low burial rate is only second to that at a high burial rate (Fig. 7A, C, E), and the pressure coefficients are normal-pressure levels (Table 2). Therefore, acidic fluids can maintain better mobility in sandstones, enhancing the effectiveness of fluid–rock interaction processes.

The experimental findings from injecting meteoric freshwater (groups 1, 2, 3) confirm widespread calcite and feldspar dissolution at low burial rates (Fig. 4B, C), resulting in the highest secondary pore content and fluid ion concentration (Figs. 5; 8). The experimental results of injecting organic acids show (groups 4, 5, 6) that, accompanied by the enhancement of mechanical compaction, the secondary pore content and fluid ion concentration decreased at low burial rates. However, they remain higher compared to medium and high burial rates (Figs. 5; 8). These observations suggest that organic acids exhibit their strongest dissolution capacity at low burial rates in the deep layer (Fig. 14).

In addition, by comparing the secondary pore contents and fluid ion concentrations of experiments in groups 1 and 4 (Figs. 5; 8), we found that the capacity of increasing pores by the dissolution of shallow layer-meteoric freshwater is stronger than that of deep layer-organic acid at low burial rates (Fig. 14). Previous studies have shown that meteoric freshwater can reach maximum depths of 2.0 km and flow velocities of 200–5000 m/yr (Giles, 1987; Bjørlykke and Jahren, 2012). These experimental results give us insight that the lower the burial rate of sandstone sediments and the longer the time in conditions with shallow layers and low temperatures may be more conducive to sandstone reservoirs accumulating more enhanced secondary pores during meteoric freshwater leaching.

4.2.3. *Negative burial rate (tectonic uplift)*

In Section 4.2.2, we realised the strong capability of increasing secondary pores by meteoric freshwater dissolution at a low burial rate. Compared to low burial rates, the ability to enlarge pores through meteoric freshwater dissolution is notably enhanced at negative burial rates. The experimental results show that the sandstone permeability appeared to have a significant ‘rebound’ under the influence of the negative burial rate, and the capacity of fluid mobility reaches its peak (Fig. 6). Therefore, compared to a low burial rate, more meteoric freshwater can move smoothly in the pore throats of sandstone sediments at a negative burial rate. Simultaneously, in an open diagenetic system with a large-scale meteoric freshwater supply, the dissolution reactions of different minerals are independent without mutual constraints (Fig. 12, Yuan et al., 2017b; Cao et al., 2022). Therefore, under negative burial rates, feldspars had adequate dissolution caused by meteoric freshwater and could even form mould pores (Fig. 4P). The concentration of each ion also reaches its peak (Fig. 8).

It is worth noting that negative burial rates can also cause the temperature of sandstone reservoirs to decrease continuously. Therefore, unstable minerals would theoretically have higher equilibrium constants for chemical reactions. The time required for dissolution–precipitation to reach equilibrium would be longer, facilitating more unstable minerals to be dissolved by meteoric freshwater, especially minerals with small equilibrium constants of chemical reaction, such as calcite (Figs. 4P; 14). Fig. 8 shows that the Ca^{2+} concentration at a negative burial rate is approximately twice as high as at a low burial rate.

4.2.4. *Medium burial rate*

Dissolution was inhibited to the maximum extent at medium burial rates for some reasons, including the following: (1) At the same simulation time, the increasing rate of temperature at medium burial rates is much higher than that at low burial rates, which leads to a continuous decrease in the equilibrium constants of the chemical reactions of unstable minerals and shortened the time of dissolution–precipitation to reach equilibrium, which is unfavourable to the continuous dissolution of minerals. (2) The dissolution capacity of acidic fluids depends on their scale and mobility (Giles, 1987). Mechanical compaction at medium burial rates causes the most significant damage to sandstone pore throat structures, which can drastically reduce the fluid mobility, scale and dissolution capacity of acidic fluids in sandstones. (3) The weakened seepage capacity also leads to difficulties in bringing dissolution products out of the dissolution zone, leading to an increase in the amount of authigenic mineral precipitation (Lander and Bonnell, 2010; Yuan et al., 2015b; Yuan et al., 2019).

Injecting meteoric freshwater (groups 1, 2, 3, 7) indicates that at low and negative burial rates, the secondary pore content is two and three times higher than at medium burial rates, except for high burial rates. Additionally, the concentration of all ions in the fluid is greater than that at medium burial rates (Figs. 5; 8). Furthermore, it is notable that the distribution area of calcite at medium burial rates significantly expands following meteoric freshwater dissolution (Fig. 4D). This diagenetic phenomenon is attributed to combining the three unfavourable factors mentioned earlier. (1) The equilibrium constant of the chemical reaction of calcite dissolution is 3–5 orders of magnitude lower than that of feldspar at the same temperature (Cao et al., 2022). Therefore, during the continued increase in temperature and the gradual closure in the

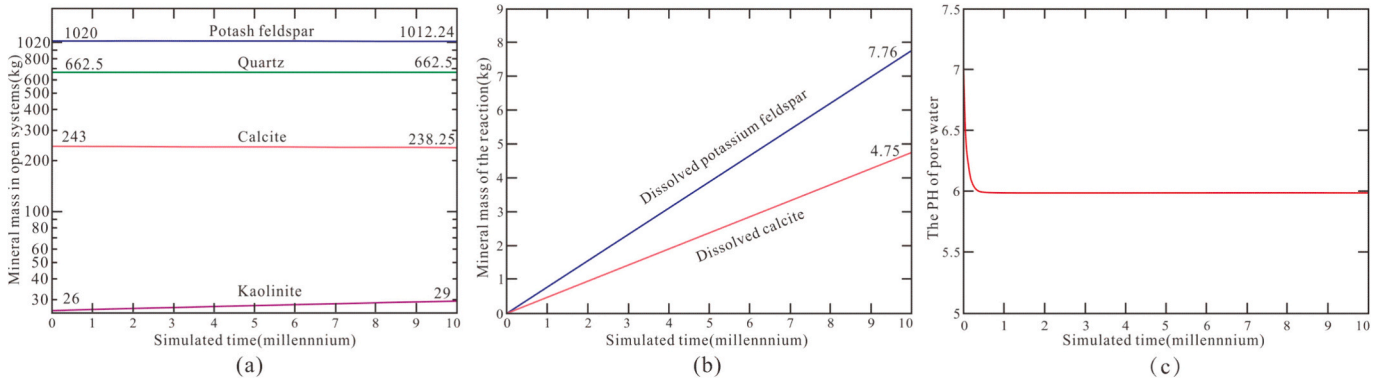

Fig. 12. The change characteristics of fluid pressure in each group of experiments. Numerical simulation results of dissolution of feldspar and calcite in sandstones by CO_2-charged fresh water with 100 times of pore water volume in 10,000 years under the open system (modified from Yuan et al., 2015a and Yuan et al., 2017b).

diagenetic system, feldspar dissolution would consume more acidic fluids such as CO_2, leading to an increase in the concentration and activity of HCO_3^-, resulting in the inhibition of calcite dissolution or even reverse precipitation. (2) The fluid seepage capacity in the closed diagenetic system is very poor, leading to Ca^{2+} generated from calcite dissolution not being efficiently removed from the dissolution zone and precipitated in situ. Previous numerical simulations have shown that feldspar and calcite undergo dissolution by acidic fluids in 1 m^3 of sandstone and lose 10.7 kg of feldspar after 1000 years. In contrast, calcite gained 1.85 kg more (Fig. 13).

$$2CaCO_3(\text{calcite}) + CO_2(g) + H_2O \rightleftarrows Ca^{2+} + 2HCO_3^- \quad (1)$$

$$KAlSi_3O_8(\text{K-feldspar}) + CO_2(g) + 1.5H_2O \rightleftarrows 0.5Al_2Si_2O_5(OH)_4(\text{kaolinite}) + 2SiO_2(\text{quartz}) + K^+ + HCO_3^- \quad (2)$$

The experimental results of injecting organic acids show (groups 4, 5, 6) that the secondary pore content and fluid ion concentration of sandstone are at their lowest values at medium burial rates (Fig. 5; Fig. 8). This situation indicates that the closure of the sandstone diagenetic system at medium burial rates is relatively strongest in deep layers, and the mineral dissolution caused by organic acids is extremely weak. Concurrently, the sandstone fluid almost loses its seepage capacity in extremely closed diagenetic systems, making it difficult to take the dissolution products out of the dissolution zone. Fig. 4 shows that authigenic kaolinite was found in sandstones with medium burial rates (Fig. 4K). In contrast, the remaining experiments did not find authigenic kaolinite (Fig. 4). In summary, at the medium burial rate, dissolution not only provides very few secondary pores for sandstones, but dissolution products occupy the existing reservoir space of sandstones very easily, which enhances the tightness of sandstones.

4.3. Implication and significance

This study establishes the connection between burial rate and sandstone diagenesis with the help of diagenetic physical simulation experiments, revealing the significance of different levels of burial rate on the quality of sandstone reservoirs, which helps to improve the understanding of the formation mechanism and distribution law of high-quality sandstone reservoirs.

This study suggests that whether or not burial rates can induce fluid overpressure is a critical factor in determining diagenetic response characteristics. Suppose the increase in burial rate can induce fluid overpressure, the damage of sandstone reservoirs caused by mechanical compaction can be inhibited. The results of the simulation experiments show that overpressure environments appear only in sandstones at high burial rates. This situation implies that on geological time scales, resisting mechanical compaction by pore fluid pressure may be more relatively obvious for sandstones at a burial rate of hundreds of metres/million years. Suppose the increase in burial rate cannot induce fluid overpressure. In that case, the mechanical compaction strength increases with an increasing burial rate. Therefore, the lower the burial rate for sandstone reservoirs with normal pressure, the lower the burial rate is, the less damage to the reservoir is caused by mechanical compaction. When the burial rate is negative (tectonic uplift), the destruction of reservoir space caused by mechanical compaction may even stop entirely and lead to a 'rebound effect' in the primary pore volume. For dissolution, if the increase in burial rate can induce fluid overpressure, then although the number of secondary pores is limited, the dissolution products are not easy to precipitate; if it does not induce fluid overpressure, then the dissolution strength is shown to be

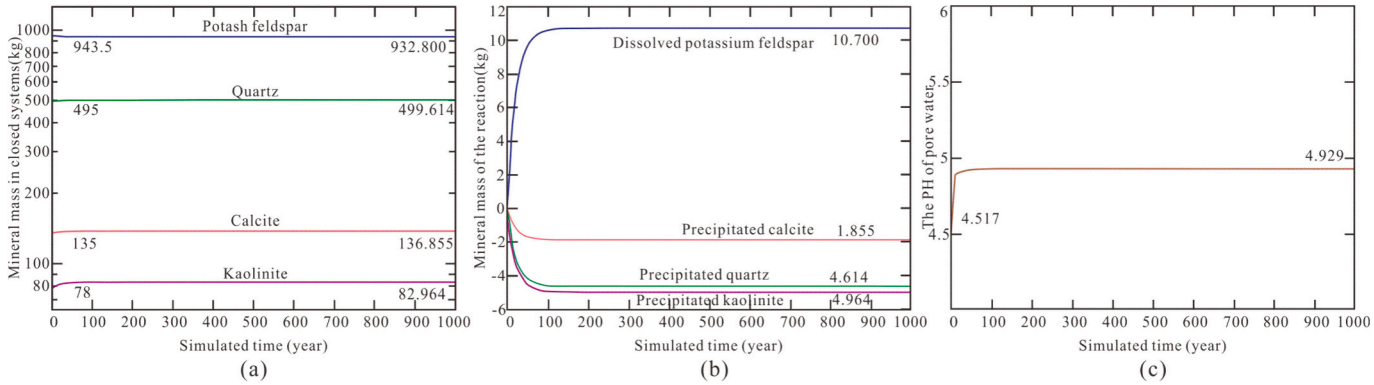

Fig. 13. Numerical simulation results of dissolution of potash feldspar and calcite in sandstones by organic acid under closed system (modified from Yuan et al., 2015a and Yuan et al., 2017b).

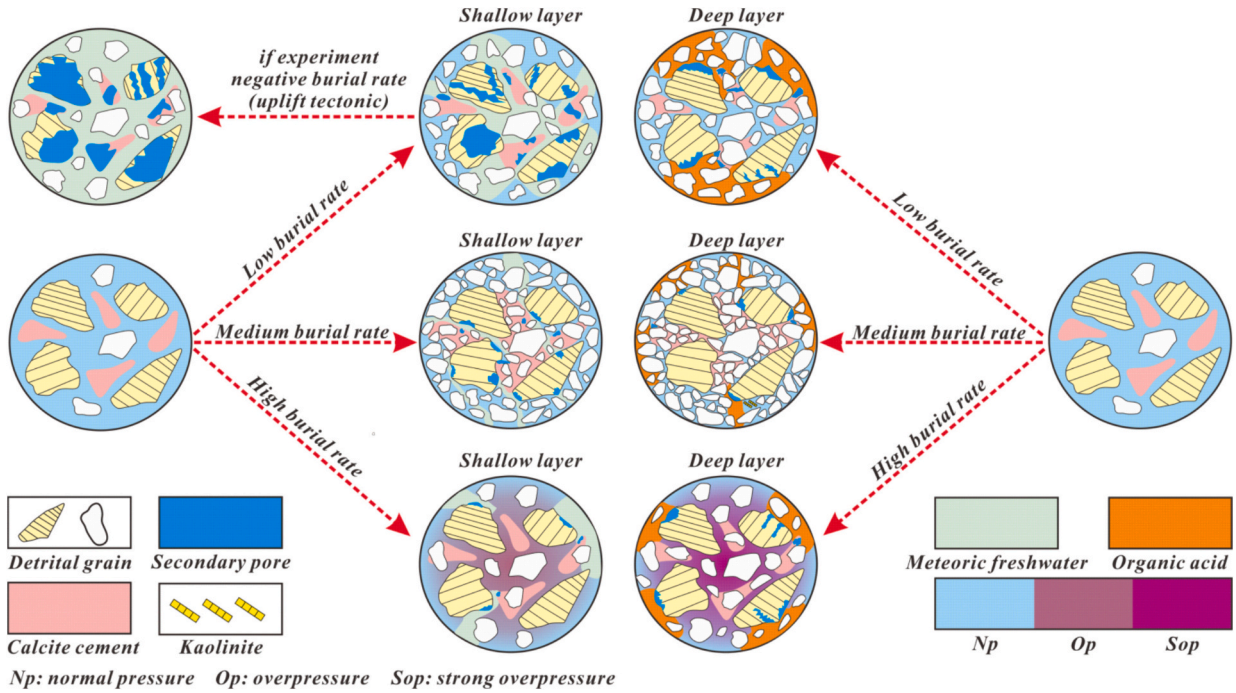

Fig. 14. Schematic diagram of influence of different burial rates on dissolution of sandstone reservoirs.

drastically weakened with the increase in burial rate. The number of secondary pores is small, and the dissolution products are easy to precipitate. Therefore, the lower (even negative) the burial rate for sandstone reservoirs with normal pressure is, the more favourable it is for dissolution to continue.

For traditional oil–gas exploration, we need to perform laboratory analyses on many cores to obtain accurate information about the diagenesis and reservoir space characteristics of sandstone reservoirs. Yet, there are no assurances of collecting cores during every underground drilling operation. However, the results of this research offer some mitigation to this issue. In regions with limited core samples, analysing the precise trends in sandstone burial rates can indirectly assist in understanding underground reservoir characteristics. Similarly, comparing burial rate trends can help predict sandstone reservoir diagenetic patterns in areas with similar geological backgrounds but varying burial histories.

However, it is important to note that the "compaction" discussed in this study is strictly "vertical compaction". Therefore, the understanding obtained in this study is more suitable for the prediction and evaluation of sandstone reservoirs in a lateral compression-undeveloped or underdeveloped petroliferous basin. In petroliferous basins with lateral compression backgrounds, horizontal and vertical compaction may coexist in sandstones, leading to a more complicated influence of burial rate on diagenesis of sandstones. Consequently, we will carry out targeted physical simulation experiments for petroliferous basins with strong lateral compression activities to perfect the study of the relationship between burial rate and sandstone diagenesis in the subsequent research.

5. Conclusion

(1) At high burial rates, pore fluid pressure indicates strong overpressure, leading to a closed diagenetic system in sandstones. Conversely, pore fluid pressure is normal at low and medium burial rates, resulting in a closed diagenetic system. Under negative burial rates, pore fluid pressure remains normal, fostering an open diagenetic system in sandstone.

(2) Mechanical compaction is weakest at high burial rates, with relatively minimal damage to primary pores, followed by low burial rates, and mechanical compaction is strongest at medium burial rates, with relatively maximum destruction of primary pores. If the burial rate of sandstone is negative, then the destruction of primary pores by mechanical compaction has almost stopped, and the primary pore content may 'rebound'.

(3) Dissolution at negative and low burial rates is strong and provides many secondary pores to the sandstone. In contrast, dissolution at medium and high burial rates is weak. Dissolution provides a limited number of secondary pores for the sandstone. In particular, at a medium burial rate, dissolution cannot provide enhanced secondary pores for sandstones, and the dissolution products occupy the existing reservoir space extremely easily, aggravating the degree of densification.

(4) The implication of this study for oil–gas exploration in sandstones is that the preliminary prediction of the development law in pore fluid pressure, diagenesis and reservoir space of sandstones can be achieved by comparing the burial rate change trend of sandstones when the difference in burial process is obvious but other macroscopic geological backgrounds are similar.

CRediT authorship contribution statement

Sirui Chen: Writing – original draft, Methodology, Investigation, Formal analysis, Data curation, Conceptualization. **Benzhong Xian:** Validation, Supervision, Resources, Project administration, Conceptualization, Visualization, Writing – review & editing. **Youliang Ji:** Supervision, Validation, Visualization. **Jiaqi Li:** Data curation, Formal analysis, Investigation. **Naveed Ur Rahman:** Formal analysis, Investigation. **Rongheng Tian:** Investigation, Methodology. **Pengyu Wang:** Formal analysis, Investigation.

Declaration of competing interest

The authors declare that they have no known competing financial interests or personal relationships that could have appeared to influence the work reported in this paper.

Data availability

The authors do not have permission to share data.

Acknowledgments

This work was supported by the National Natural Science Foundation of China (No. 42172109, 41872113, 42172108), China National Petroleum Corporation - China University of Petroleum (Beijing) strategic cooperation science and technology project (ZLZX2020-02), State's Key Project of Research and Development Plan (2018YFA0702405) and Science Foundation of China University of Petroleum (Beijing) (No. 2462020BJRC002, 2462020YXZZ020).

References

Aschwanden, L., Diamond, L.W., Adams, A., 2019. Effects of progressive burial on matrix porosity and permeability of dolostones in the foreland basin of the Alpine Orogen, Switzerland. Mar. Pet. Geol. 100, 148–164. https://doi.org/10.1016/j.marpetgeo.2018.10.055.

Baig, I., Faleide, J.I., Mondol, N.H., Jahren, J., 2019. Burial and exhumation history controls on shale compaction and thermal maturity along the Norwegian North Sea basin margin areas. Mar. Pet. Geol. 104, 61–85. https://doi.org/10.1016/j.marpetgeo.2019.03.010.

Baruch, E.T., Kennedy, M.J., Lohr, S.C., Dewhurst, D.N., 2015. Feldspar dissolution-enhanced porosity in Paleoproterozoic shale reservoir facies from the Barney Creek Formation (McArthur Basin, Australia). AAPG Bull. 99, 1745–1770. https://doi.org/10.1306/04061514181.

Bjørlykke, K., Jahren, J., 2012. Open or closed geochemical systems during diagenesis in sedimentary basins: Constraints on mass transfer during diagenesis and the prediction of porosity in sandstone and carbonate reservoirs. AAPG Bull. 96, 2193–2214. https://doi.org/10.1306/04301211139.

Bloch, S., Lander, R.H., Bonnell, L., 2002. Anomalously high porosity and permeability in deeply buried sandstone reservoirs: Origin and predictability. AAPG Bull. 86, 301–328. https://doi.org/10.1306/61EEDABC-173E-11D7-8645000102C1865D.

Cao, Y.C., Yuan, G.H., Wang, Y.Z., Zan, N.M., Jin, Z.H., Liu, K.Y., Xi, K.L., Wei, Y.H., Sun, P.P., 2022. Successive formation of secondary pores via feldspar dissolution in deeply buried feldspar-rich clastic reservoirs in typical petroliferous basins and its petroleum geological significance. Sci. China Earth Sci. 65, 1673–1703. https://doi.org/10.1007/s11430-020-9931-9.

Chen, L., Ji, H.C., Zhang, L., Jia, H.B., Zhu, Y., Fang, Z., 2017. Effect of burial processes on the evolution of organic acids and implications for acidic dissolution from a case study of the Nanpu Sag, Bohai Bay Basin, China. J. Nat. Gas Sci. Eng. 39, 173–187. https://doi.org/10.1016/j.jngse.2017.01.020.

Chuhan, F., Kjeldtad, A., Bjørlykke, K., Høeg, K., 2002. Porosity loss in sand by grain crushing—experimental evidence and relevance to reservoir quality. Mar. Pet. Geol. 19, 39–53. https://doi.org/10.1016/S0264-8172(01)00049-6.

Curtis, C.D., 1980. Diagenetic alteration in black shales. J. Geol. Soc. Lond. 137, 189–194. https://doi.org/10.1144/gsjgs.137.2.0189.

Dixon, S.A., Summers, D.M., Surdam, R.C., 1989. Diagenesis and preservation of porosity in norphlet formation (Upper Jurassic), Southern Alabama. AAPG Bull. 73, 707–728. https://doi.org/10.1306/44B4A24E-170A-11D7-8645000102C1865D.

Dutton, S.P., Loucks, R.G., 2010. Diagenetic controls on evolution of porosity and permeability in lower Tertiary Wilcox sandstones from shallow to ultradeep (200-6700m) burial, Gulf of Mexico Basin, U.S.A. Mar. Pet. Geol. 27, 69–81. https://doi.org/10.1016/j.marpetgeo.2009.12.010.

França, A.B., Araújo, L.M., Maynard, J.B., Potter, P.E., 2003. Secondary porosity formed by deep meteoric leaching: Botucatu eolianite, southern South America. AAPG Bull. 87, 1073–1082. https://doi.org/10.1306/02260301071.

Fu, Y., Luo, J.L., Shi, X.F., Cao, J.J., Mao, Q.R., Sheng, W.Y., 2022. Implications of lithofacies and diagenetic evolution for reservoir quality: a case study of the Upper Triassic chang 6 tight sandstone, southeastern Ordos Basin, China. J. Pet. Sci. Eng. 218, 111051 https://doi.org/10.1016/j.petrol.2022.111051.

Giles, M.R., 1987. Mass transfer and problems of secondary porosity creation in deeply buried hydrocarbon reservoirs. Mar. Pet. Geol. 4, 188–204. https://doi.org/10.1016/0264-8172(87)90044-4.

Glasmann, J.R., 1992. The fate of feldspar in Brent Group reservoirs, North Sea: a regional synthesis of diagenesis in shallow, intermediate, and deep burial environments. Geol. Soc. Lond. Spec. Publ. 61, 329–350. https://doi.org/10.1144/GSL.SP.1992.061.01.17.

Hansen, H.N., Løvstad, K., Lageat, G., Clerc, S., Jahren, J., 2021. Chlorite coating patterns and reservoir quality in deep marine depositional systems – example from the cretaceous Agat Formation, Northern North Sea, Norway. Basin Res. 33, 2725–2744. https://doi.org/10.1111/bre.12581.

Hao, F., Zou, H.Y., Ni, J.H., Zeng, Z.P., Wang, M.J., 2002. Evolution of overpressured systems in sedimentary basins and conditions for deep oil/gas accumulation. Earth Sci. 27, 610–615 (in Chinese with English Abstract).

Hui, W., Wang, Y.S., Ren, D.Z., Hui, J., 2020. Effects of pore structures on the movable fluid saturation in tight sandstones: a He8 formation example in Sulige Gasfield, Ordos Basin, China. J. Pet. Sci. Eng. 192, 107295 https://doi.org/10.1016/j.petrol.2020.107295.

Jin, F.M., Zhang, K.X., Wang, Q., Niu, X.J., Yu, Z.G., Bai, G.P., Zhao, X., 2018. Formation mechanisms of good-quality clastic reservoirs in deep formations in rifted basins: a case study of Raoyang sag in Bohai Bay Basin, East China. Pet. Explor. Dev. 45, 264–272. https://doi.org/10.1016/S1876-3804(18)30029-6.

Karimi, A.R., Rabbani, A.R., Kamali, M.R., 2016. A bulk kinetic, burial history and thermal modeling study of the Albian Kazhdumi and the Eocene-Oligocene Pabdeh formations in the Ahvaz anticline, Dezful Embayment, Iran. J. Pet. Sci. Eng. 146, 61–70. https://doi.org/10.1016/j.petrol.2016.04.015.

Lander, R.H., Bonnell, L.M., 2010. A model for fibrous illite nucleation and growth in sandstones. AAPG Bull. 94, 1161–1187. https://doi.org/10.1306/04211009121.

Leder, F., Park, W., 1986. Porosity reduction in sandstone by Quartz overgrowth. AAPG Bull. 70, 1713–1728. https://doi.org/10.1306/94886CA4-1704-11D7-8645000102C1865D.

Li, D., Dong, C.M., Lin, C.Y., Ren, L.H., Jiang, T., Tang, Z.X., 2013. Control factors on tight sandstone reservoirs below source rocks in the Rangzijing slope zone of southern Songliao Basin, East China. Pet. Explor. Dev. 40, 742–750. https://doi.org/10.1016/S1876-3804(13)60099-3.

Li, J., Zhao, J.Z., Wei, X.S., Chen, M.N., Song, P., Han, Z.H., Wu, W.T., 2019. Origin of abnormal pressure in the Upper Paleozoic shale of the Ordos Basin, China. Mar. Pet. Geol. 110, 162–177. https://doi.org/10.1016/j.marpetgeo.2019.07.016.

Li, J., Zhao, J.Z., Wei, X.S., Shang, X.Q., Wu, W.T., Wu, H.Y., Chen, M.N., 2022. Gas expansion caused by formation uplifting and its effects on tight gas accumulation: a case study of Sulige gas field in Ordos Basin, NW China. Pet. Explor. Dev. 49, 1266–1281. https://doi.org/10.1016/S1876-3804(23)60348-9.

Ma, X.H., Xie, J., Yong, R., Zhu, Y.Q., 2020. Geological characteristics and high production control factors of shale gas reservoirs in Silurian Longmaxi Formation, southern Sichuan Basin, SW China. Pet. Explor. Dev. 47, 901–915. https://doi.org/10.1016/S1876-3804(20)60105-7 (Marine and Petroleum Geology).

Ma, Z.L., Tan, J.Q., Zheng, L.J., Ni, C.H., Hu, R.N., Ma, J.F., 2022. Simulation experiment of fluid-feldspar sandstone interactions and their implications for tight oil and gas exploration of the Yanchang Formation, Ordos Basin, China. Mar. Pet. Geol. 142, 105737 https://doi.org/10.1016/j.marpetgeo.2022.105737.

Morad, S., Al-Ramadan, K., Ketzer, J.M., De Ros, L.F., 2010. The impact of diagenesis on he heterogeneity of sandstone reservoirs: a review of the role of depositional facies and sequence stratigraphy. AAPG Bull. 94, 1267–1309. https://doi.org/10.1306/04211009178.

Osborne, M.J., Swarbrick, R.E., 1999. Diagenesis in North Sea HPHT clastic reservoirs consequences for porosity and overpressure prediction. Mar. Pet. Geol. 16, 337–353. https://doi.org/10.1016/S0264-8172(98)00043-9.

Parks, K.P., Tóth, J., 1995. Field evidence for erosion-induced under pressuring in Upper cretaceous and Tertiary strata, west Central Alberta, Canada. Bull. Can. Petrol. Geol. 43, 281–292. https://doi.org/10.35767/gscpgbull.43.3.281.

Poursoltani, M.R., Gibling, M.R., Pe-Piper, G., 2019. Diagenesis, burial history, and hydrocarbon potential of Cambrian sandstone in the northern continental margin of Gondwana: a case study of the Lalun Formation of Central Iran. J. Asian Earth Sci. 172, 143–169. https://doi.org/10.1016/j.jseaes.2018.09.003.

Qu, X.Y., Zhang, Y.C., Chen, X., Yang, X.B., You, L., Zhong, J., 2020. Physical simulation experiment on porosity evolution and controlling factors of Miocene reservoir in Ledong-Lingshui Depression, Qiongdongnan Basin, South China Sea. Arab. J. Geosci. 13, 1022. https://doi.org/10.1007/s12517-020-05956-w.

Saha, A., Bhattacharya, B., 2022. Controls on near-surface and burial diagenesis of a syn-rift siliciclastic rock succession: a study from Permian Barren measures formation, Southern India. Sediment. Geol. 436, 106170 https://doi.org/10.1016/j.sedgeo.2022.106170.

Salama, A.M., Abd-Allah, Z.M., El-Sayed, M.I., 2021. Source rock evaluation and burial history modeling of cretaceous rocks at the Khalda Concession of Abu Gharadig Basin, Western Desert, Egypt. J. Afr. Earth Sci. 184, 104372 https://doi.org/10.1016/j.jafrearsci.2021.104372.

Sathar, S., Jones, S., 2016. Fluid overpressure as a control on sandstone reservoir quality in a mechanical compaction dominated setting: Magnolia Field, Gulf of Mexico. Terra Nova 28, 155–162. https://doi.org/10.1111/ter.12203.

Sun, L.D., Zou, C.N., Zhu, R.K., Zhang, Y.H., Zhang, S.C., Zhang, B.M., Zhu, G.Y., Gao, Z.Y., 2013. Formation, distribution and potential of deep hydrocarbon resources in China. Pet. Explor. Dev. 40, 687–695. https://doi.org/10.1016/S1876-3804(13)60093-2.

Teng, J.B., Qiu, L.W., Zhang, S.P., Ma, C.F., 2022. Origin and diagenetic evolution of dolomites in Paleogene Shahejie Formation lacustrine organic shale of Jiyang Depression, Bohai Bay Basin, East China. Pet. Explor. Dev. 49, 1251–1265. https://doi.org/10.1016/S1876-3804(23)60347-7.

Tenger, B., Lu, L.F., Yu, L.J., Zhang, W.T., Pan, A.Y., Shen, B.J., Wang, Y., Yang, Y.F., Gao, Z.W., 2021. Formation, preservation and connectivity control of organic pores in shale. Pet. Explor. Dev. 48, 798–812. https://doi.org/10.1016/S1876-3804(21)60067-8.

Wang, W.G., Lin, C.Y., Zhang, X.G., Dong, C.M., Ren, L.H., Lin, J.L., 2020. Effect of burial history on diagenetic and reservoir-forming process of the Oligocene sandstone in Xihu sag, East China Sea Basin. Mar. Pet. Geol. 112, 104034 https://doi.org/10.1016/j.marpetgeo.2019.104034.

Wang, X., He, S., Jones, S.J., Yang, R., Wei, A.J., Liu, C.H., Liu, Q., Cheng, C.Y., Liu, W.M., 2019. Overpressure and its positive effect in deep sandstone reservoir quality of Bozhong Depression, offshore Bohai Bay Basin, China. J. Pet. Sci. Eng. 182, 106362 https://doi.org/10.1016/j.petrol.2019.106362.

Worden, R.H., Benshatwan, M.S., Potts, G.J., Elgarmadi, S.M., 2016. Basin-scale fluid movement patterns revealed by veins: Wessex Basin, UK. Geofluids 16, 149–174. https://doi.org/10.1111/gfl.12141.

Xi, K.L., Cao, Y.C., Wang, Y.Z., Zhang, Q.Q., Jin, J.H., Zhu, R.K., Zhang, S.M., Wang, J., Yang, T., Du, L.H., 2015. Factors influencing physical property evolution in

sandstone mechanical compaction: the evidence from diagenetic simulation experiments. Pet. Sci. 12, 391–405. https://doi.org/10.1007/s12182-015-0045-6.

Yang, L.L., Xu, T.F., Liu, K.Y., Peng, B., Yu, Z.Z., Xu, X.M., 2016. Fluid–rock interactions during continuous diagenesis of sandstone reservoirs and their effects on reservoir porosity. Sedimentology 64, 1303–1321. https://doi.org/10.1111/sed.12354.

Yuan, G.H., Cao, Y.C., Jia, Z.Z., Gluyas, J., Yang, T., Wang, Y.Z., Xi, K.L., 2015a. Selective dissolution of feldspars in the presence of carbonates: the way to generate secondary pores in buried sandstones by organic CO_2. Mar. Pet. Geol. 60, 105–119. https://doi.org/10.1016/j.marpetgeo.2014.11.001.

Yuan, G.H., Cao, Y.C., Gluyas, J., Li, X.Y., Xi, K.L., Wang, Y.Z., Jia, Z.Z., Sun, P.P., Oxtoby, N.H., 2015b. Feldspar dissolution, authigenic clays, and quartz cements in open and closed sandstone geochemical systems during diagenesis: typical examples from two sags in Bohai Bay Basin, East China. AAPG Bull. 99, 2121–2154. https://doi.org/10.1306/07101514004.

Yuan, G.H., Cao, Y.C., Zhang, Y.C., Gluyas, J., 2017a. Diagenesis and reservoir quality of sandstones with ancient “deep” incursion of meteoric freshwater—an example in the Nanpu Sag, Bohai Bay Basin, East China. Mar. Pet. Geol. 82, 444–464. https://doi.org/10.1016/j.marpetgeo.2017.02.027.

Yuan, G.H., Cao, Y.C., Gluyas, J., Jia, Z.Z., 2017b. Reactive transport modeling of coupled feldspar dissolution and secondary mineral precipitation and its implication for diagenetic interaction in sandstones. Geochim. Cosmochim. Acta 207, 232–255. https://doi.org/10.1016/j.gca.2017.03.022.

Yuan, G.H., Cao, Y.C., Schulz, H.M., Hao, F., Gluyas, J., Liu, K.Y., Yang, T., Wang, Y.Z., Xi, K.L., Li, F.L., 2019. A review of feldspar alteration and its geological significance in sedimentary basins: from shallow aquifers to deep hydrocarbon reservoirs. Earth Sci. Rev. 191, 114–140. https://doi.org/10.1016/j.earscirev.2019.02.004.